FEATURE ARTICLE

Water Dynamics: Vibrational Echo Correlation Spectroscopy and Comparison to Molecular Dynamics Simulations

John B. Asbury,[†] Tobias Steinel,[†] C. Stromberg,[†] S. A. Corcelli,[‡] C. P. Lawrence,[‡] J. L. Skinner,[‡] and M. D. Fayer*,[†]

Department of Chemistry, Stanford University, Stanford, California 94305, and Department of Chemistry, University of Wisconsin, Madison, Wisconsin 53706

Received: August 2, 2003; In Final Form: November 5, 2003

The dynamics of water are examined using ultrafast IR stimulated vibrational echo correlation spectroscopy. The OD hydroxyl stretch of HOD in H_2O is probed with 45-fs pulses that have sufficient bandwidth (>400 cm^{-1}) to span the entire broad spectrum. High-quality 2D correlation spectra are obtained having the correct phase relations across the broad hydroxyl band. The correlation spectra are found to evolve on multiple time scales. The time evolution of the vibrational echo correlation spectrum reflects the structural evolution of the hydrogen bond networks. The extended vibrational lifetime of the OD hydroxyl stretch of HOD in H_2O facilitates the measurement of hydrogen bond dynamics for longer times than possible in previous studies of the OH stretch. Molecular dynamics simulations/electronic structure calculations are used to obtain the time correlation functions (TCF) for two water models, TIP4P and SPC/E. The TCFs are inputs to full time-dependent diagrammatic perturbation theory calculations, which yield theoretical correlation spectra. Quantitative comparison with the data demonstrates that the two water models somewhat overemphasize the fast fluctuations in water and do not contain a slow enough component to account for the slowest fluctuations. Fits to the data using a phenomenological triexponential TCF yield a slowest component of ∼2 ps, and TIP4P and SPC/E have slowest components of <1 ps. The TCF obtained from the water models and the triexponential TCF reproduce the linear absorption line shape equally well, but all miss to some extent the asymmetric "wing" on the low-energy side of the line. Therefore, the time dependence of the vibrational echo correlation spectra provides a good test for the TCF, but the absorption spectrum does not.

I. Introduction

Water is ubiquitous in nature. It has profound effects on diverse fields of science from astronomy to zoology. The properties of water are dominated by the strong hydrogen bonds that form among water molecules. The hydrogen bonds give rise to hydrogen bonding networks that play a major role in both the structure and dynamics of water.[1−9] The hydrogen bond networks are continually evolving in time. Hydrogen bonds break, and new hydrogen bonds form. Structural evolution causes weak hydrogen bonds to become strong and strong hydrogen bonds to become weak.

Properties of hydrogen bond networks can be studied using IR spectroscopy of the hydroxyl stretching mode because of the influence of the number of hydrogen bonds and the strength of hydrogen bonds on the hydroxyl stretching frequency.[10−13] A water molecule can form up to four hydrogen bonds, and the various types and number of hydrogen bonds are not spectroscopically resolvable under the broad hydrogen-bonded hydroxyl stretching band.[12,13]

Vibrational echo correlation spectroscopy of the hydroxyl stretch examines the time evolution of the hydroxyl stretching frequency and, therefore, the hydrogen bonds themselves. Very strong evidence for the correlation between the hydroxyl stretching frequency and the hydrogen bond strength in solids is obtained from correlating crystallographic and spectroscopic data.[11] From the crystallographic data, the length of the hydrogen bond can be determined. A shorter length corresponds to a stronger bond. Observations of a large number of compounds show that as the bond shortens the hydroxyl stretching frequency shifts to the red. The fact that the crystallographic/spectroscopic relationship also applies to liquids follows from three observations about the hydroxyl stretch of hydrogen-bonded liquids, such as water and alcohols. First, molecules that form stronger hydrogen bonds display larger red shifts in their hydroxyl stretch than molecules that form weak hydrogen bonds.[10,14,15] There is general agreement in the literature that the red side of the hydroxyl stretch of a hydrogen-bonding liquid corresponds to stronger hydrogen bonds.[3,7,10,14−22] Second, the hydroxyl stretching band is inhomogeneously broadened.[7,13,21−27] In a hydrogen-bonding liquid, the lengths and strengths of hydrogen bonds vary substantially, giving rise to the broad, inhomogeneously broadened hydroxyl stretching band.[12] Finally, the hydroxyl

* Corresponding author. E-mail: fayer@stanford.edu.
[†] Stanford University.
[‡] University of Wisconsin.

10.1021/jp036266k CCC: $27.50
Published on Web 01/10/2004

stretching frequency of water varies continuously from its low-temperature, icelike spectrum (large red shift, strong hydrogen bonds) to its high-temperature, vaporlike spectrum (small red shift, weak hydrogen bonds) when the temperature is varied from the freezing to boiling points.[3] Falk and Ford concluded that hydrogen bonds varied continuously in strength rather than having a fixed strength.[3] The stronger hydrogen bonds correspond to the red side of the hydroxyl stretch because the red side is lost when the temperature is raised. Similar behavior has been observed in methanol over a limited temperature range.[24,28,29]

Recently, there has been an increase in understanding of hydrogen-bonding liquids brought about by the application of ultrafast IR experimental methods, particularly a variety of transient absorption experiments.[16−19,28−35] The development of the ultrafast IR vibrational echo technique[36−39] and the recent extension to multidimensional vibrational echo methods[23−25,40−49] provide a new approach for the study of condensed matter systems. Such techniques are beginning to be applied to hydrogen-bonding systems.[23−25,45,50,51] The structure and evolution of hydrogen-bonding networks have been extensively studied by molecular dynamics (MD) simulations.[8,12,13,52−55]

Here we report the first application of ultrafast heterodyne-detected multidimensional stimulated vibrational echo correlation spectroscopy with full phase information to the study of the dynamics of water. The OD hydroxyl stretch of low-concentration HOD in H_2O is studied. The extended vibrational lifetime of the OD hydroxyl stretch ($\sim$1.8 ps)[30,56−58] facilitates the measurement of hydrogen bond dynamics for longer times compared with previous studies[7,16−19,21,22,27,50,59] that focused on the OH stretch (lifetime $<$ 1 ps).[7,9,18,35,60] Hydrogen bond breaking occurs later in the dynamics following the excitation of the OD stretch,[56] which greatly simplifies the analysis of the slower hydrogen bond dynamics. By using ultrashort mid-IR pulses (45 fs or $\sim$3.4 cycles of light), it is possible to perform experiments on the entire broad hydroxyl stretching band despite its $>$400-cm^{-1} width. Employing pulses that are transform-limited and controlling path lengths with the accuracy of a small fraction of a wavelength of light, along with proper data analysis, data are obtained with correct phase relationships across the entire spectrum. The proper phase relationships permit the accurate separation of the absorptive and dispersive contributions to the spectra.[23,25,43,44,49,61] As a result, the 2D IR correlation spectra are obtained in a manner akin to 2D NMR spectroscopy.[62]

The multidimensional stimulated vibrational echo correlation spectroscopy technique measures the population and vibrational dephasing dynamics in two frequency dimensions, ω_τ and ω_m.[23,25,43,44,46,49,61] (In NMR, ω_τ and ω_m are usually called ω_1 and ω_3, respectively.[62]) The ω_m axis is similar to the frequency axis in frequency-resolved pump−probe spectroscopy. The ω_τ axis does not have an analogue in the pump−probe experiment; it provides an additional dimension of information that is contained only in the correlation spectrum. The positions and signs of peaks in the correlation spectra contain the history of the various vibrational transitions involved in the experiment. The time evolution of the shapes of the peaks provides information on the dynamics of the system produced by the structural evolution of the hydrogen-bonding network.

MD simulations[8,12,13,54] specifically performed for the OD stretch of HOD in water are used in the data analysis. The coupling to the OD oscillator uses a new approach involving electronic structure calculations on water clusters. The simulations yield the time correlation function (TCF). The TCFs are inputs to full time-dependent diagrammatic perturbation theory calculations, which yield theoretical correlation spectra. The diagrammatic treatment uses the TCF to obtain the line shape function that has real and imaginary contributions. The imaginary portion accounts for the time-dependent Stokes shift. The line shape function is then used to obtain the response functions employed in the calculations of the correlation spectra. Calculations were performed for two of the most widely used water models, TIP4P[63] and SPC/E.[64] Comparisons of the experimental vibrational echo correlation spectra to the MD-derived theoretical correlation spectra provide a stringent test of the water models. In addition, the experimental data were fit using a phenomenological triexponential TCF. The results show that the two water models somewhat overemphasize the fast fluctuations in water and do not contain a slow enough component to account for the slowest structural fluctuations. Fits to the data using the phenomenological triexponential TCF yield a slowest component of 2 ps, and TIP4P and SPC/E have slowest components of $<$1 ps. The TCF obtained from the water models and the triexponential TCF reproduce the linear absorption line shape equally well, but all miss to some extent the asymmetric "wing" on the low-energy side of the line. Therefore, the time dependence of the vibrational echo correlation spectra provides a good test for the TCF, but the absorption spectrum does not.

II. Vibrational Echo Correlation Spectroscopy and Experimental Procedures

The ultrashort IR pulses employed in the experiments are generated using a Ti:sapphire regeneratively amplified laser/OPA system. The output of the modified Spectra Physics regen is 26-fs transform-limited $^2/_3$-mJ pulses at a 1-kHz rep rate. These are used to pump a substantially modified Spectra Physics short-pulse IR OPA. The output of the OPA is compressed to produce 45-fs transform-limited IR pulses as measured by collinear autocorrelation. For the experiments, the compression was readjusted to give 45-fs transform-limited pulses in the sample as measured by a sample that gave a purely nonresonant signal. The shot-to-shot IR stability is $\sim$1.0%, and the long-term stability is such that data were collected continuously for as long as 5 days.

The IR beam is split into five beams. Three of the beams are the excitation beams for the stimulated vibrational echo. A fourth beam is the local oscillator (LO) used to heterodyne detect the vibrational echo signal. One of the excitation beams is also used for pump−probe experiments, and the fifth beam is the probe beam in the pump−probe experiments. All of the beams that pass through the sample are optically identical and are compensated for GVD simultaneously. The vibrational echo signal combined with the LO is passed through a monochromator and detected by a 32-element MCT array. At each monochromator setting, the array detects 32 individual wavelengths.

The sample, 5% HOD in H_2O, was held in a sample cell of CaF_2 flats with a spacing of 6 μm. The peak absorbance of the samples was 0.2. Such a low absorbance is necessary to prevent serious distortions of the pulses as they propagate through the sample. The OD stretch of HOD is used as a probe of water for three reasons. The relatively dilute OD stretch reduces the rate of vibrational excitation transport to the point where transport has a negligible influence on the dynamics.[31] Excitation transport would be a source of spectral diffusion that is not related to the structural dynamics of water. Furthermore, it is very difficult to have a pure water sample that is thin enough to

have the necessary low optical density for the experiments, and such a thin sample is subject to heating artifacts. Finally, the longer vibrational lifetime of the OD stretch of HOD in H_2O ($\sim$1.8 ps)[30,56−58] compared to the OH-stretch lifetime (<1 ps)[7,9,18,35,60] allows us to monitor the dynamics in water twice as long without the complication of hydrogen bond breaking.[23−26,28,29,45,51,56]

The phase-resolved, heterodyne-detected, stimulated vibrational echo was measured as a function of one frequency variable, ω_m, and two time variables, τ and T_w, that are defined as the time between the first and second sample−radiation field interactions and the second and third sample−radiation field interactions, respectively. The measured signal is the absolute value squared of the sum of the vibrational echo signal electric field, S, and the local oscillator electric field, L:

$$|L + S|^2 = L^2 + 2LS + S^2 \quad (1)$$

The L^2 term is time-independent, and the S^2 term is very small; hence neither contributes to the time dependence of the signal. The $2LS$ term is the heterodyne amplified signal. The monochromator performs an experimental Fourier transform on the radiation. Through data processing that involves chopping to measure L^2 and normalization, the spectrum yields the ω_m frequency axis. As the τ variable is scanned in 2-fs steps, the phase of the vibrational echo signal electric field is scanned relative to the fixed local oscillator electric field, resulting in an interferogram measured as a function of the τ variable. The interferogram contains the amplitude, sign, frequency, and phase of the vibrational echo signal electric field as it varies with τ. By numerical Fourier transformation, this interferogram is converted into the frequency variable ω_τ, providing the ω_τ axis.

The interferogram measured as a function of τ contains both the absorptive and dispersive components of the vibrational echo signal. However, two sets of quantum pathways can be measured independently by appropriate time ordering of the pulses in the experiment.[43,44,61] With pulses 1 and 2 at the time origin, pathway 1 or 2 is obtained by scanning pulse 1 or 2 to negative time, respectively. Adding the Fourier transforms of the interferograms from the two pathways, the dispersive component cancels, leaving only the absorptive component. The 2D vibrational echo correlation spectra are constructed by plotting the amplitude of the absorptive component as a function of both ω_m and ω_τ.

The lack of perfect knowledge of the timing of the pulses and the consideration of chirp on the vibrational echo pulse requires a "phasing" procedure to be used.[23,25] The projection slice theorem is employed to generate the absorptive 2D correlation spectrum.[23−25,43−45,61,62] The projection of the absorptive 2D correlation spectrum onto the ω_m axis is equivalent to the IR pump−probe spectrum recorded at the same T_w, as long as all of the contributions to the stimulated vibrational echo are absorptive. Consequently, a comparison of the projected 2D stimulated vibrational echo spectrum to the pump−probe spectrum permits the correct isolation of the absorptive vibrational echo correlation spectrum from the 2D spectrum obtained from the addition of the two quantum pathways.

It is possible to come relatively close to the correct correlation spectrum prior to the "phasing" procedure because the very short pulses permit their time origins to be known within a few femtoseconds. However, the correlation spectrum is very sensitive to small errors in the time origin, even on the order of 1 fs, and to chirp. Therefore, a well-defined phasing procedure based on various potential errors was developed.[23,25] The frequency-dependent phasing factor used to correct the 2D spectra has the form

$$S_C(\omega_m, \omega_\tau) = S_1(\omega_m, \omega_\tau)\,\Phi_1(\omega_m, \omega_\tau) + S_2(\omega_m, \omega_\tau)\,\Phi_2(\omega_m, \omega_\tau)$$

$$\Phi_1(\omega_m, \omega_\tau) = \exp[i(\omega_m \Delta\tau_{LO,E} + \omega_\tau \Delta\tau_{1,2}) + \omega_m \omega_\tau C + \omega_m{}^2 Q] \quad (2)$$

$$\Phi_2(\omega_m, \omega_\tau) = \exp[i(\omega_m \Delta\tau_{LO,E} - \omega_\tau \Delta\tau_{1,2}) + \omega_m \omega_\tau C + \omega_m{}^2 Q]$$

S_C is the correlation spectrum. S_1 and S_2 are the spectra recorded for pathways 1 and 2, respectively. $\Delta\tau_{LO,E}$ accounts for the lack of perfect knowledge of the time separation of the LO pulse and the vibrational echo pulse; $\Delta\tau_{1,2}$ accounts for the lack of perfect knowledge of the time origins of excitation pulses 1 and 2; C accounts for linear chirp caused by the echo propagating through the sample; and Q accounts for the linear chirp caused by the propagation of the vibrational echo through the back window of the sample cell. $\Delta\tau_{1,2}$ comes in with opposite signs for pathways 1 and 2. A more detailed description of the phasing procedure, including the experimental minimization of $\Delta\tau_{LO,E}$, $\Delta\tau_{1,2}$, and C, has been published elsewhere.[25]

An additional procedure was developed and employed to produce the very high quality correlation spectra shown below. The projection slice theorem reduces a 2D entity to a 1D entity. In many instances, this is sufficient.[43,44,61] However, to assign a correct correlation spectrum unambiguously, it is preferable to use information from both dimensions. Therefore, in the phasing procedure an additional constraint is applied for the ω_τ dimension.[25] We can use information from the absolute value correlation spectrum, which is the sum of the absolute value spectra of pathway 1 (rephasing) and pathway 2 (nonrephasing) discussed above. The absolute value spectrum is independent of the phase factor and peaks at the same frequency along ω_τ as the purely absorptive spectrum. Consequently, the difference in peak positions of a trial phased absorptive spectrum and the absolute value spectrum for each ω_m gives an additional criterion for the quality of the correlation spectrum. The correct correlation spectrum is the one that provides the best fit to the pump−probe spectrum *and* minimizes the difference in peak positions of absorptive and absolute value spectra. This procedure holds for symmetric line shapes and hence can be applied to the data discussed here, where the dynamical lines can be very well fit to a Gaussian line shape and the small deviations are symmetric. Following phasing, the errors in the time origins are $<100 \times 10^{-18}$ s, and the time shift across the entire spectrum due to chirp, $\omega_m C$, is $<100 \times 10^{-18}$ s.

III. Results and Discussion

A. Vibrational Echo Correlation Spectra. The vibrational echo correlation spectra displayed in Figure 1 are 2D frequency maps of the dynamics of the OD stretch. The ω_τ axis (horizontal axis) displays the frequency of the interaction of the sample with the first laser pulse. Water exists predominantly in its hydroxyl-stretch ground vibrational state (level 0) at room temperature. Consequently, the first interaction occurs between the ground and first excited vibrational state (level 1). The 0−1 transition frequency of the OD stretch of HOD occurs at $\sim$2500 cm^{-1}. Examining the correlation spectra in Figure 1, we find that all of the features appear to be centered at the 0−1 transition frequency along the ω_τ axis. The ω_m axis displays the frequency at which the vibrational echo was emitted from the sample. In

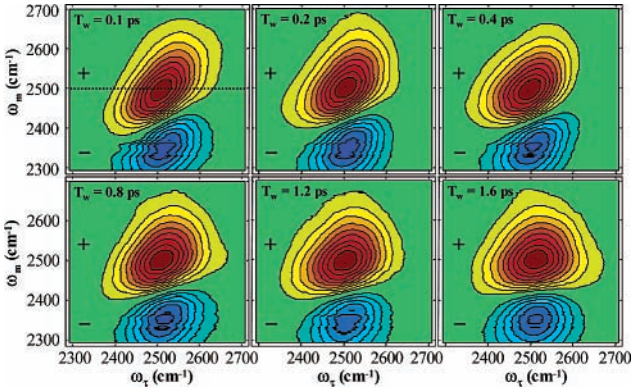

Figure 1. Experimental vibrational echo correlation spectra of the OD stretch of HOD in H_2O. Each contour represents a 10% change. The positive-going peak arises from the 0−1 transition. The negative-going peak arises from the 1−2 transition. The 0−1 and 1−2 peaks are elongated along the diagonal, indicating that inhomogeneity persists in the hydroxyl stretching frequency distribution. Spectral diffusion broadens the widths of the peaks as T_w increases.

vibrational echo correlation spectroscopy, the ground state and the first and second vibrational excited states are accessed. Consequently, two peaks are observed along the ω_m axis corresponding to the 0−1 and the 1−2 transition frequencies. The positive-going peak, corresponding to the radiation emitted at the 0−1 transition frequency, appears on the diagonal (represented by the line $\omega_m = \omega_\tau$) because the vibrational echo is emitted with the same frequency as the first interaction with the radiation field (first pulse). The negative-going peak, corresponding to the vibrational echo emitted at the 1−2 transition frequency, appears red-shifted along the ω_m axis by the anharmonicity, Δ_{an}. The anharmonic potential of the hydroxyl stretch results in a lower frequency for the 1−2 than for the 0−1 transition. The vibrational echo was emitted on the 1−2 transition, but the first interaction was on the 0−1 transition. Consequently, the 1−2 peak appears off-diagonal at ($\omega_m = \omega_{0-1} - \Delta_{an}$, $\omega_\tau = \omega_{0-1}$). Similar to the situation in IR pump−probe spectroscopy, the 0−1 peak is positive, and the 1−2 peak is negative because they result from a decrease in the ground-state population and an increase in the excited-state population, respectively.

The correlation spectra in Figure 1 are displayed at T_w delays of 100, 200, 400, 800, 1200, and 1600 fs. Starting at the earliest T_w delay ($T_w = 100$ fs), we find that the 0−1 and 1−2 peaks appear to be elongated along the diagonal because their widths along the ω_τ axis are smaller than their total width (observed by looking at the projection of the peak on the ω_m axis). The width of the 0−1 peak along the ω_τ axis is the dynamical line width.[65,66] (Note that we employ a procedure described below to ensure that we specifically extract the dynamical line width of the 0−1 transition.) Because the hydroxyl stretch of HOD is inhomogeneously broadened for small T_w, the resulting band shapes are asymmetric.[65,66] As T_w increases, the widths of the 0−1 and 1−2 peaks along the ω_τ axis broaden. The broadening along the ω_τ axis is progressive, monotonically increasing as T_w increases. By $T_w = 1600$ fs, the width of the 0−1 peak along the ω_τ axis grows toward its asymptotic value. Detailed calculations (described below) show that the width of the 0−1 peak approaches but does not reach its asymptotic limit by 1.6 ps.

Changes in the dynamical line width report the spectral diffusion dynamics[12,26,58,67−70] occurring in the hydroxyl stretching peak of water.[12,26] A detailed analysis of the dynamical line widths will be presented below. Qualitatively, the change in the dynamical line width can be seen by looking at a cross-sectional cut of the 0−1 peak at a particular ω_m value and projecting it onto the ω_τ axis. The horizontal dashed line shown in the $T_w = 100$ fs panel of Figure 1 illustrates such a cut at the apparent center of the hydroxyl stretching peak at 2500 cm^{-1}. It is clear that as T_w increases the 0−1 band changes shape and the 2500-cm^{-1} cut becomes broader. The dynamical line measured in the correlation spectra of HOD is narrow when spectral diffusion has not randomized the distribution of hydroxyl stretching frequencies. As spectral diffusion occurs, the dynamical line width broadens. Because the hydroxyl stretching frequency is correlated with the number and strength of hydrogen bonds, the time evolution of the vibrational echo correlation spectra reflects the evolution of the hydrogen-bonding network.

The time dependence of the dynamical line width measured by vibrational echo correlation spectroscopy is equivalent to performing a transient hole-burning experiment that covers the entire line, and because it is done in the time domain, vibrational echo correlation spectroscopy does not have a time−bandwidth product limitation. As will be discussed in another publication, the ω_m dependence of the dynamical line width can be used to address the question of the inhomogeneity of dynamics across the very broad water absorption band.[71]

As T_w increases, the peak shape changes, and the amplitude of the emitted vibrational echo also decreases because of excited-state relaxation. The data displayed in Figure 1 have been normalized to the amplitude of the 0−1 peak, which obscures the amplitude decay. The signal amplitude actually decays by a factor of ∼3 over the time period displayed because the lifetime of the OD stretch is 1.8 ± 0.2 ps.[30,56−58] Water and other hydrogen-bonding liquids are known to break hydrogen bonds following excitation and vibrational relaxation of the hydroxyl stretch.[20,28,29,60,72−77] Because we want to study the hydrogen bond dynamics of water and not the photoproducts of hydrogen bond breaking, it necessary to restrict our observation window to less than the vibrational lifetime. We have performed detailed, spectrally resolved IR pump−probe experiments and find that hydrogen bond breaking does not contribute significantly to the spectrum for pump−probe delays of <2 ps.[56] Consequently, we consider only correlation spectra measured at T_w delays of <2 ps to simplify the analysis. We have measured correlation spectra and pump−probe spectra at T_w delays of >2 ps. The hydrogen bond dynamics and further spectral diffusion dynamics will be discussed in detail in a future publication.

The above discussion pinpoints a significant advantage of using the OD stretch of HOD in H_2O to study hydrogen bond dynamics over using the OH stretch of HOD in D_2O.[7,16−19,21,22,27,50,59] In addition to studying water rather than D_2O, the vibrational lifetime of the OH stretch of HOD in D_2O is <1 ps.[7,9,18,35,60] Because hydrogen bonds break following the vibrational relaxation of the hydroxyl stretch,[23−26,28,29,45,51,56] the hydrogen-bond-broken species will come to dominate the vibrational echo or transient hole-burning signals measured for the OH stretch in D_2O much faster than in studies of the OD stretch in H_2O. On the basis of the comparison of the vibrational lifetimes, we expect the products of hydrogen bond breaking to dominate the echo or THB signals in ∼1 ps, making the quantitative measurement of the frequency fluctuations in water (not the photoproduct) extremely difficult for time scales longer than 1 ps.[22−25,45,51,56] Our recent IR pump−probe study and vibrational echo correlation spectra collected at T_w delays of >2 ps indicate that water molecules on the low-frequency side

of the hydroxyl stretching peak preferentially break hydrogen bonds, similar to the behavior observed in MeOD.[23−25,45,51,56] Consequently, the time window is limited to <1 ps for experimental investigations of the frequency fluctuations in water that use the OH stretch of HOD in D_2O to probe the dynamics, unless modeling procedures are employed to model both the initially excited species and the products of hydrogen bond breaking. Most investigators neglected this complication in the analysis of their results[7,16−19,21,50,59] and hence may have included artifacts that influenced their assignment of the slow component of the fluctuations in water.

B. Semiclassical MD Simulations and the TCFs. Changes in the dynamical line width report the time scales and amplitudes of the frequency fluctuations that cause the spectral diffusion of the OD hydroxyl stretch because the OD stretch senses the dynamics of the water in which it is embedded. Thus, the dynamical line width reports the effects of the frequency fluctuations that are described by the time correlation function (TCF). (Note that the time correlation function is frequently referred to as the frequency−frequency correlation function.) The TCF is defined as

$$C(t) = \langle \delta\omega(t)\, \delta\omega(0) \rangle \tag{3}$$

where $\delta\omega$ is the change in the hydroxyl stretching frequency from its average value. The TCF describes the loss of correlation of the frequency of an ensemble of OD stretches as time progresses from $t = 0$, the time of the first interaction, to $t = T_w$, approximately the time that the echo is emitted. As the structure of the hydrogen-bonding network evolves, the frequency of a given OD oscillator will change. The TCF describes the "randomization" of the OD oscillators' frequencies throughout the entire absorption line. At sufficiently long time, a given oscillator may be found at any frequency in the absorption spectrum, independent of its initial frequency.

The TCF is the input for the calculation of the theoretical vibrational echo correlation spectrum. The full third-order nonlinear material response using diagrammatic perturbation theory including finite pulse durations is determined to correlate the time dependence of the correlation spectrum and the TCF[46−48] quantitatively. Comparing the dynamical line width of the experimentally observed vibrational echo correlation spectra with the dynamical line width extracted from calculations based on the underlying TCF makes it possible to test the accuracy of the dynamics predicted by models of water and to "fit" the data to extract a phenomenological TCF. The methods we use to compare the dynamics predicted from MD simulation with the experimentally observed dynamics are described in detail below. Briefly, (1) a particular water model simulation is implemented, and (2) the TCF for a given model of water is generated from methods that involve electronic structure calculations and classical MD simulations. (3) We calculate the vibrational echo correlation spectra from the TCF using time-dependent diagrammatic perturbation theory to obtain the full third-order nonlinear material response.[47] (4) We extract the change in the dynamical line width and compare to the experimental data. This comparison provides a stringent test of the water models, which allows us to test our understanding of water dynamics quantitatively. In fitting the data, we begin at (3) using a phenomenological triexponential TCF based on the results obtained from the water models.

Two methods for calculating the normalized TCF for the OD stretch of HOD in H_2O have been used. The first method has been described in detail for the OH stretch of the HOD/D_2O system.[12,13,54] It begins with an accurate quantum mechanical Hamiltonian for the gas-phase HOD molecule[78] and the classical TIP4P model for the H_2O molecules.[63] The total Hamiltonian is separated into a term for the quantum mechanical vibrations of the HOD molecule (the "system"), a term for the rest of the degrees of freedom (the "bath"), and a term for the system−bath coupling. The system Hamiltonian is then renormalized by the average interaction with the bath. The fluctuating OD stretching frequency is obtained from diagonal matrix elements (between eigenstates of the system Hamiltonian) of the system−bath coupling. These matrix elements are classical bath variables, so a trajectory of the fluctuating frequency can then be obtained from a classical molecular dynamics simulation. From this trajectory, the TCF is calculated.

The second method[79] is very different in spirit and is based on ab initio electronic structure calculations of clusters of molecules. First, configurations of molecules are generated from a classical molecular dynamics simulation of the HOD/H_2O system. Then a representative set of HOD$(H_2O)_n$ clusters are extracted from the simulation. For each cluster, a series of ab initio calculations (using density functional theory) are performed for different values of the OD stretching coordinate, and in doing so, a potential curve that leads to an anharmonic 0−1 OD transition frequency for the HOD molecule in that cluster is generated. From looking at 100 or so clusters, it was determined that there is a linear correlation between the OD frequency and the component of the electric field from the H_2O molecules on the D atom in the direction of the OD bond vector (correlation coefficient = 0.89). Assuming that this same linear correlation holds for the full liquid, the normalized TCF simply becomes the normalized electric field time correlation function. The latter can be generated easily from a completely classical molecular dynamics simulation.

The second method[79] was first applied to the TIP4P model for HOD/H_2O. The results for the normalized TCF are very similar to those obtained with the first method described here. For the second method, the simulation was actually performed on the neat H_2O system because in that way much better statistics can be obtained by averaging over all molecules. It was determined that this change makes a negligible difference. With this new method, it is very easy to examine other water models, and in this paper, we also report results specifically for the OD stretch of SPC/E HOD in H_2O.[64]

The TCFs obtained from MD simulation are fit with exponential functions to obtain an analytical representation. The numerical TCFs can be represented exceedingly well with the sum of exponentials. Calculations with the numerical TCFs generated by the simulations produced indistinguishable correlation spectra from those generated with the exponential fits. However, considerable calculation time was saved using the analytical forms. These functions have the form

$$C(t) = \Delta_0^2 \exp\left(-\frac{t}{\tau_0}\right) + \Delta_1^2 \exp\left(-\frac{t}{\tau_1}\right) + \Delta_2^2 \exp\left(-\frac{t}{\tau_2}\right) \tag{4}$$

Whereas the time constants in eq 4 were obtained directly from the simulations, the magnitudes of the prefactors were not able to reproduce the linear absorption line shape (see below). The ratios of the prefactors were maintained, but they were multiplied by a constant to reproduce the full width at half-maximum of the experimentally measured absorption spectrum. The triexponential representations of the TCFs produced from the three models of water are displayed in Figure 2. We will henceforth refer to the triexponential fit as the TCF. The TCFs have been normalized to unit magnitude at time $t = 0$. The two TIP4P models are extremely similar, being dominated by a fast

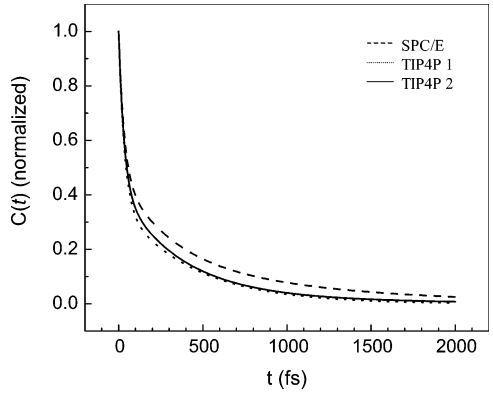

Figure 2. Triexponential fits to the MD simulation-derived TCFs corresponding to the TIP4P and SPC/E models of water. Two methods are used from the TIP4P simulations that give almost identical results (see text).[12,79] The SPC/E model displays a slow component. The parameters for the triexponential functions are given in Table 1.

TABLE 1: TCF Parameters[a]

TCF	Δ_0 (rad/ps), (%)	τ_0 (ps)	Δ_1 (rad/ps), (%)	τ_1 (ps)	Δ_2 (rad/ps), (%)	τ_2 (ps)
tri-exp. fit	11.5, (43)	0.032	4.2, (16)	0.4	10.8, (41)	1.8
SPC/E	12.1, (52)	0.031	9.0, (29)	0.28	7.4, (19)	0.98
TIP4P	13.0, (58)	0.032	10.2, (36)	0.34	4.4, (6)	0.90

[a] See eq 4.

component with a time constant of ∼30 fs and a slower component of ∼500 fs. Because the two TIP4P TCFs are virtually identical, below we will consider only one of them, the one obtained from the second MD simulation method described above. Parameters for the two water model TCFs are summarized in Table 1 along with a phenomenological TCF we obtained by a fitting procedure to be described below. As displayed in Figure 2, the TCF from the SPC/E model displays somewhat slower dynamics than the TIP4P model. The slow component of this TCF has a time constant of ∼1 ps with ∼19% of the total amplitude. Although the time constant of the slowest component in the TIP4P TCF, 0.9 ps, is similar, it has significantly less amplitude. The fact that the two methods for the determination of the TIP4P TCF give almost identical results indicates that differences in the TIP4P and SPC/E TCFs arise from differences in the water models rather than from some aspect of the coupling to the OD stretching frequency.

From the TCFs, we calculate the linear line shape as the first step in comparing the theoretical with the experimental correlation spectra. The calculated linear line shapes for the TCFs discussed in this work are compared with the experimentally measured linear line shape (measured by FTIR spectroscopy) in Figure 3. From MD simulation, we obtain normalized TCFs, which describe the time scales and relative amplitudes of the frequency fluctuations but not the absolute magnitude of those fluctuations. We calculate the time domain line-shape function, $g(t)$, from the TCF, $C(t)$, with the assumption of Gaussian fluctuations,[47]

$$g(t) = \int_0^t \int_0^{t_2} C(t_1)\, \mathrm{d}t_1\, \mathrm{d}t_2 - \mathrm{i}\lambda \int_0^t \left[1 - \frac{C(t_1)}{C(0)}\right] \mathrm{d}t_1 \quad (5)$$

where 2λ is the reorganization energy. In the high-temperature limit, λ is related to Δ_{tot} by

$$\lambda = \frac{\hbar \Delta_{\mathrm{tot}}^2}{2 k_{\mathrm{B}} T} \quad (6)$$

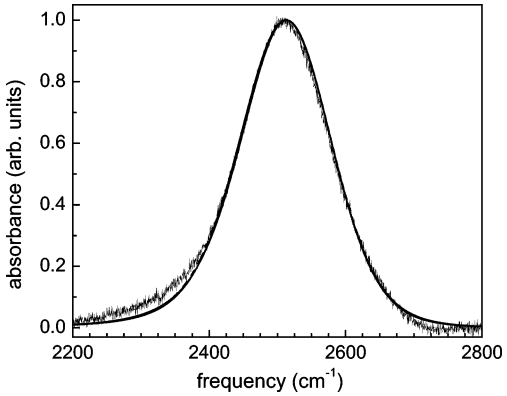

Figure 3. Comparison of the linear line shape calculated from the three TCFs to the experimentally measured linear line shape of the OD stretch of HOD in H_2O. The TCFs produce good descriptions of the linear line shape but miss the red wing to some extent. The calculated spectra from the TCFs are virtually indistinguishable from each other. A Gaussian fit to the experimental spectrum yields a 162-cm^{-1} fwhm.

where Δ_{tot}^2 is defined in terms of eq 4 by

$$\Delta_{\mathrm{tot}}^2 = \Delta_0^2 + \Delta_1^2 + \Delta_2^2 \quad (7)$$

The reorganization energy is included in the calculations because it makes a small but nonnegligible contribution. The linear line shape, $I(\Omega)$, is then calculated from $g(t)$ by[47]

$$I(\Omega) = \frac{1}{\pi} \mathrm{Re}\left[\int_0^\infty \mathrm{d}t \exp(-\mathrm{i}(\Omega - \omega_0)t) \exp(-g(t))\right] \quad (8)$$

where ω_0 is the center of the transition. The detailed shape of the linear line is determined from the functional form of the TCF and by the initial amplitude, Δ_{tot}^2 (see eqs 4 and 7). Therefore, the normalized TCFs are multiplied by a scaling factor to obtain the correct linear line width. The amplitudes of the prefactors, Δs, listed in Table 1 for each TCF reflect the appropriate scaling to reproduce the linear line shape. (Note that Δ_{tot}^2 is not the linear line width. One or more contributions from the TCF may be motionally narrowed, and the linear line width is the convolution of the various components.) As can be seen in Figure 3, all of the TCFs reproduce the linear line shape with equal accuracy. The calculated curves are indistinguishable. The calculated line shapes are not symmetrical. There is a wing to the low-energy side, but it is not sufficient to reproduce the wing in the experimental absorption spectrum accurately. The low-energy wing in the experimental linear spectrum arises from the combined effects of the Stokes shift that is determined by the reorganization energy, 2λ, which is estimated to be ∼35 cm^{-1} from eq 6, and potentially non-Gaussian frequency fluctuations.[13,80,81] The calculated linear lines are systematically unable to reproduce the low-energy wing in the linear spectrum either because eq 6 underestimates the Stokes shift or because the fluctuations are not Gaussian. The diagrammatic perturbation theory implicitly assumes Gaussian fluctuations and so cannot describe the influence of non-Gaussian fluctuations.[46,47,82]

We calculate the theoretical vibrational echo correlation spectra from the appropriately scaled TCFs using diagrammatic perturbation theory to obtain the third-order nonlinear material response.[46,47,82] The line shape function given in eq 5 is used to obtain the response functions, R_i.[46,47,82] Because the bandwidth of the laser is large enough to cover both the 0−1 and 1−2 transitions of the hydroxyl stretch and we determine the

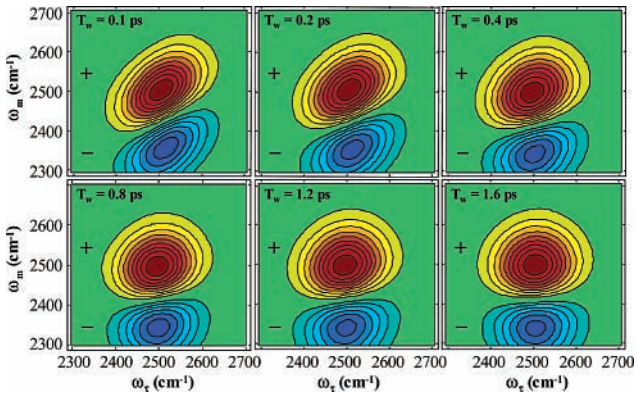

Figure 4. Simulated vibrational echo correlation spectra calculated from the TCF that is derived from the SPC/E model of water. Each contour represents a 10% change. The simulated correlation spectra show the same qualitative features as the experimental spectra (see Figure 1). The 0−1 is positive-going and the 1−2 peak is negative-going. The peaks are elongated along the diagonal for short T_w delays. As T_w increases, the peaks broaden along the ω_τ (horizontal) axis.

absorptive component of the vibrational echo, a total of 16 response functions (quantum pathways) must be considered.[47,83−86] To account for finite-duration pulses in the calculations, time-ordered integrations over the response functions are used to generate the final third-order polarization

$$P^{(3)}(\tau, T_w, \tau_s) = \int_0^\infty \int_0^\infty \int_0^\infty \sum_i R_i(t_3, t_2, t_1)$$

$$*E_1^*(\tau_s + \tau + T_w - t_3 - t_2 - t_1)\, E_2(\tau_s + T_w - t_3 - t_2)\, E_3(\tau_s - t_3)\, dt_1\, dt_2\, dt_3 \quad (9)$$

where the E_i are the electric fields of the three laser pulses

$$E_i(t) = e^{i\mathbf{k_i}\cdot\mathbf{r} - i\omega_i t} e^{-t^2/2\sigma^2} \quad (10)$$

τ_s is the time variable associated with the emitted vibrational echo pulse. The third-order polarization is then Fourier transformed along the τ and τ_s dimensions to give frequency−frequency plots (ω_τ, ω_m) that can be compared to the correlation spectra.

Two separate calculations are performed to obtain each correlation spectrum corresponding to the positive and negative τ scan experiments (pathways 1 and 2 respectively, see section II). Once the positive and negative τ calculations have been performed, the results can be manipulated in the same manner as the experimental data to generate the calculated correlation spectra. The only difference is the absence of the phasing procedure for the calculated spectra.

Representative theoretical correlation spectra calculated using the TCF obtained from the SPC/E model of water are shown in Figure 4 at the values of T_w for which the experimental correlation spectra were collected. The correlation spectra for the TIP4P model of water have a similar appearance. The parameters of the triexponential function describing the TCF, from which these correlation spectra were calculated, are given in Table 1. The theoretical correlation spectra show the same qualitative features as the experimental spectra. The 0−1 peak appears on the diagonal, and the 1−2 peak appears shifted off-diagonal by the anharmonicity. In this calculation, we assumed an anharmonicity of 140 cm^{-1} based on best fits of the IR pump−probe data (not shown) and the experimental correlation spectra (displayed in Figure 1). The uncertainty in the measurement of the anharmonicity is ±20 cm^{-1}. The calculations have been normalized to the amplitude of the 0−1 peak. The 0−1 peak in the T_w = 100 fs correlation spectrum displays the characteristic elongation along the diagonal that demonstrates the presence of inhomogeneity in the hydroxyl stretching peak. In Figure 4, as T_w increases, the shape of the 0−1 peak changes, reflecting the increasing dynamical line width. The theoretical correlation spectra display significant changes to the dynamical line in the first few hundred femtoseconds. After 800 fs, they display only small changes.

C. Comparison of Experimental and Theoretical Correlation Spectra. A comparison of the experimental and calculated correlation spectra is difficult to present in the 2D representation using contour plots. The data and calculations may be more clearly compared using the dynamical line widths obtained from each set. This method makes it possible to construct a simple plot to compare the data and calculations, which facilitates their quantitative comparison in a clear and concise manner. This discussion corresponds to step (4) of the analysis scheme discussed in section III.B. The dynamical line shape cannot be obtained directly by taking a cross-sectional cut out of the data at a particular ω_m to get a spectrum with respect to ω_τ. The cross-sectional cut out of the data at the center of the hydroxyl stretching peak, ω_m = 2500 cm^{-1} (see Figure 1, T_w = 100 fs, dashed line), is influenced to a small degree by the negative 1−2 peak because the two features overlap. The overlap of the two features at ω_m = 2500 cm^{-1} decreases as the dynamical line width increases. Consequently, the dynamical line width as a function of the T_w delay can be obtained more accurately from the data by first fitting the 2D spectra.

We employed a model in which the sum of two 2D Gaussian peak shapes of opposite sign were used to fit both the 0−1 and 1−2 peaks of the experimental and theoretical correlation spectra for each T_w delay. The sum of the two 2D Gaussian peaks has the form

$$S(\omega_m, \omega_\tau) = \{[A_{0-1} \exp(-(\cos(\theta)(\omega_m - \omega_{m,0-1}) + \sin(\theta)(\omega_\tau - \omega_{\tau,0-1}))^2/2\sigma_{d,0-1}^2) * \exp(-(\sin(\theta)(\omega_{m,0-1} - \omega_m) + \cos(\theta)(\omega_\tau - \omega_{\tau,0-1}))^2/2\sigma_{a,0-1}^2)] \quad (11)$$

$$- [A_{1-2} \exp(-(\cos(\theta)(\omega_m - \omega_{m,1-2}) + \sin(\theta)(\omega_\tau - \omega_{\tau,1-2}))^2/2\sigma_{d,1-2}^2) * \exp(-(\sin(\theta)(\omega_{m,1-2} - \omega_m) + \cos(\theta)(\omega_\tau - \omega_{\tau,1-2}))^2/2\sigma_{a,1-2}^2)]\}$$

The parameters A_{0-1} and A_{1-2} describe the amplitudes of the 0−1 and 1−2 peaks, respectively. Because the data are normalized to the amplitude of the 0−1 peak, A_{0-1} is always approximately unity. The terms including the angle θ reflect a 45° coordinate transformation from the (ω_m, ω_τ) plane to the (ω_d, ω_a) plane (the plane constructed from the diagonal and antidiagonal axes). This transformation allows the diagonally elongated peak shapes to be described by a simple 2D Gaussian function. The positions $\omega_{m,0-1}$ and $\omega_{\tau,0-1}$ reflect the position of the 0−1 peak in the (ω_m, ω_τ) plane; $\omega_{m,1-2}$ and $\omega_{\tau,1-2}$ reflect the corresponding position of the 1−2 peak. The full width at half-maximum of the peaks along the diagonal are represented by $2.35\sigma_{d,0-1}$ and $2.35\sigma_{d,1-2}$; those along the antidiagonal are represented by $2.35\sigma_{a,0-1}$ and $2.35\sigma_{a,1-2}$. The square root of the laser spectrum was divided out of the experimental data along the ω_m axis to remove the influence of the local oscillator

spectrum. This procedure produces experimental correlation spectra having the same dependence on the combined spectra of the three input pulses as the calculated correlation spectra, thus allowing the same fitting procedure to be employed for both experimental and calculated correlation spectra.

The best fits to the 2D spectra are obtained by minimizing the integral over the square of the residual volume,

$$R^2 = 100 \times \frac{\int\int (S_{\mathrm{corr}}(\omega_{\mathrm{m}}, \omega_\tau) - S_{\mathrm{fit}}(\omega_{\mathrm{m}}, \omega_\tau))^2 \,\mathrm{abs}(S_{\mathrm{corr}}(\omega_{\mathrm{m}}, \omega_\tau))\, \mathrm{d}\omega_{\mathrm{t}}\, \mathrm{d}\omega_{\mathrm{m}}}{\int\int \mathrm{abs}(S_{\mathrm{corr}}(\omega_{\mathrm{m}}, \omega_\tau))^3\, \mathrm{d}\omega_{\mathrm{t}}\, \mathrm{d}\omega_{\mathrm{m}}} \quad (12)$$

resulting from subtracting the 2D Gaussian fit, $S_{\mathrm{fit}}(\omega_{\mathrm{m}}, \omega_\tau)$, from the experimental or theoretical correlation spectrum, $S_{\mathrm{corr}}(\omega_{\mathrm{m}}, \omega_\tau)$. The residual volume is weighted by the absolute magnitude amplitude of the correlation spectrum and normalized by the total volume raised to the appropriate power. This evaluation scheme emphasizes the peaks in the correlation spectrum over the wings and the area containing no signal. Much of the area in the 2D frequency map contains no signal. Small amounts of noise in these areas can grow to dominate the sum of the squares of the residuals because of the large area over which they are integrated. This problem is avoided by weighting the residuals according to eq 12. Typical best fits to the correlation spectra have residual volume errors of <0.2% of the total volume of the correlation spectrum. The fits describe both the calculated correlation spectra and the experimental correlation spectra exceedingly well. After fitting the correlation spectra, we null the amplitude of the 1−2 peak, leaving only the 0−1 peak. A cross-sectional cut of the 0−1 peak at $\omega_{\mathrm{m}} = 2500$ cm^{-1} is fit with a Gaussian. The resulting fwhm is a measure of the dynamical line width. The purpose of the model is to provide a simple, quantitative description of the calculations and the data that can be compared in a simple plot. The method allows us to extract the time evolution of the dynamical line width from the 0−1 peak without interference from the 1−2 peak. In the harmonic approximation, the 0−1 and 1−2 transitions are described by the same TCF.[43] However, this approximation may not apply in water because of the very large anharmonicity associated with the hydroxyl stretch.[54] Therefore, it is useful to separate the 0−1 and 1−2 transitions to obtain the 0−1 TCF. The results of the procedure show that the correction to the dynamical line widths at $\omega_{\mathrm{m}} = 2500$ cm^{-1} is ∼1%. However, that the correction is small could be known only by going through the procedure. For wavelengths to the red of $\omega_{\mathrm{m}} = 2500$ cm^{-1}, not analyzed here, the correction becomes larger because of increasing overlap with the 1−2 transition.

Figure 5 displays the dynamical line widths extracted from the vibrational echo correlation spectra calculated for the TIP4P and the SPC/E models and the experimental data. The dashed line at 147 cm^{-1} is the long-time asymptotic line width. This width is narrower than the absorption spectrum (162 cm^{-1} fwhm from Gaussian fit to absorption spectrum, see Figure 3) because the measured dynamical line width is the product of the true dynamical line width and the laser intensity spectrum raised to the appropriate power (∼1.5).[61] Although the pulses used in the experiment were ∼45 fs fwhm, the influence of their spectrum reduced the measured dynamical line width. Calculations demonstrate that 6-fs pulses are required for the asymptotic value of the measured dynamical line width to be indistinguishable from the absorption spectrum. The error bars on the experimental data indicate the upper and lower bounds at which R^2 (eq 12) is 2 times larger than its best-fit value. The experimental data show a clear slow component with a few picoseconds time constant that does not reach its asymptotic limit by 1.6 ps, the last data point. The dynamical line widths as a function of the T_{w} delay calculated from the theoretical correlation spectra show the same qualitative trends—a rapid increase during the first few hundred femtoseconds, followed by slower growth at larger T_{w} delays.

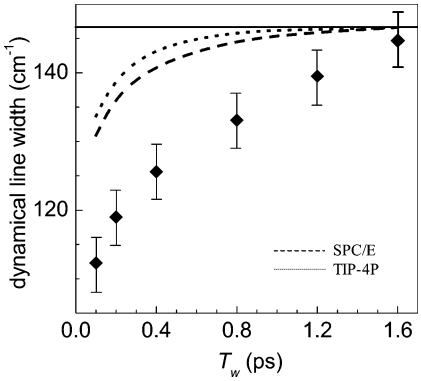

Figure 5. Comparison of the dynamical line widths of the simulated and experimental correlation spectra obtained from the 2D Gaussian fits. The experimental data appear as diamonds with error bars. The horizontal line at 147 cm^{-1} is the long-time asymptotic line width. The top curve (dots) is from the TIP4P model, and the lower curve (dashes) is from the SPC/E model. The TIP4P model has reached the asymptotic limit by 1.6 ps, but the SPC/E model approaches more slowly. Compared to the data, both models have too much amplitude at short time, and the long-time components are too fast.

A comparison of the results from the TIP4P model of water with the experimental results displayed in Figure 5 demonstrates that the TIP4P model does not accurately describe the hydrogen bond network dynamics of water that are reflected by the frequency fluctuations of the hydroxyl (OD) stretch. The dynamical line widths extracted from the correlation spectra calculated from the MD-derived TIP4P TCF overestimate the dynamical line width at $T_{\mathrm{w}} = 100$ fs by ∼20% compared with the experimental data. The TIP4P model predicts that the dynamical line width should reach its asymptotic limit by $T_{\mathrm{w}} = 1.6$ ps. The increase in the dynamical line width, which is too rapid, is a result of the middle component of the TIP4P TCF being somewhat too fast but is mainly due to the slowest component being too fast and having a small amplitude. The TCF obtained from the TIP4P model is dominated by a fast component with 58% amplitude and a slowest component (0.9 ps) with only 6% amplitude. By $T_{\mathrm{w}} = 1.6$ ps, the TCF decays to <2% of its value. By 1.6 ps, the distribution of hydroxyl stretching frequencies is virtually randomized, and the dynamical line width has broadened to essentially its maximum value (147 cm^{-1}). A comparison of the results predicted from the TIP4P model with the experimental data clearly demonstrates that these dynamics are too fast.

The SPC/E model describes the dynamics of water somewhat more accurately than the TIP4P model. The correlation spectra calculated from the MD-derived SPC/E TCF overestimate the dynamical line width at $T_{\mathrm{w}} = 100$ fs by ∼15%. The dynamical line width approaches the asymptotic value more slowly than does the TIP4P model. The TCF calculated from the SPC/E model contains a slow component comprising 19% of the amplitude in the TCF with a time constant of ∼1 ps. At $T_{\mathrm{w}} = 1.6$ ps, this component retains ∼4% of its initial value, which slows the approach of the dynamical line width to its asymptotic limit compared to the TIP4P model. The SPC/E model predicts

a larger amplitude for the slowest fluctuations in water, in contrast to the TIP4P model. Nonetheless, in comparison to the data, the SPC/E model displays dynamical broadening that is too fast. Neither the TIP4P nor the SPC/E model captures water dynamics accurately. They both have very fast dynamics contributions that are too large, and the slowest dynamics are too fast and do not have sufficient amplitude (see below). The failure of the MD simulations to reproduce the data seems to be in the water models themselves rather than in the method used to calculate the water fluctuations to the OD oscillator frequency. As shown in Figure 2, two very different methods were used to calculate the TCF for TIP4P, but the results were almost identical.

A phenomenological TCF can be obtained by fitting the dynamical line widths extracted from data using steps (3) and (4) of the analysis scheme discussed above. On the basis of the results from the water model-generated TCFs, we use a triexponential form. We begin by entering a triexponential function as the TCF into the full third-order material response calculation (eq 9). As output, we generate simulated correlation spectra, which are fit using eqs 11 and 12 to obtain the time-dependent dynamical line widths corresponding to the input TCF. This output is compared with the experimental data. We iteratively repeat steps (3) and (4) until the dynamical line widths obtained from the simulated correlation spectra best fit the experimentally observed dynamical line widths.

The parameters of the triexponential function were constrained to be consistent with other complementary experiments and calculations to obtain the greatest confidence in the parameters. Constraint of the initial magnitude of the TCF was achieved by fitting the linear absorption line shape calculated from the TCF to the absorption spectrum (see Figure 3). Therefore, the TCF reproduces the long-time asymptotic value of the measured dynamic line width, 147 cm^{-1}. One of the three indistinguishable curves displayed in Figure 3 was calculated from the phenomenological TCF. This procedure also causes the preexponential factor, Δ_i^2, of one the exponential components to be dependent on the other two. As a result, only two of the three Δ's are varied independently in the fitting procedure. The amplitudes of the Δ's in Table 1 reflect the appropriate initial magnitude to reproduce the linear line shape.

The time constant of the fast component was set equal to 32 fs to be consistent with the fast components of the TCFs obtained by MD simulation. This time scale is also consistent with recent work by Hamm and co-workers, who found that a 33-fs component of the TCF provided the best fit to their two-pulse vibrational echo measurement of water.[27] (Note that we are currently in the process of measuring the very short time scale, <100-fs correlation spectra. Even with pulses that are 45 fs, when the pulses overlap, there are additional technical and theoretical issues associated with measuring the correlation spectra. We believe that we have overcome these problems, and we will be able to test the <100-fs behavior of the TCF subsequently.) Of particular interest here is the long-time component of the TCF because the time constant and amplitude of this component are in substantial error when calculated from the water models. To reduce further the number of adjustable parameters in the fit to the data, the time constant for the intermediate component was set equal to the intermediate decay component (400 fs) in a vibrational echo peak-shift measurement that we performed in the course of these experiments. The vibrational echo peak-shift measurement has been demonstrated to reproduce the TCF[87−90] given a sufficient waiting time, T_w, so that the value of the normalized TCF is $\ll 1$.[89,90] For the vibrational echo peak-shift measurement in water to represent the TCF, the minimum waiting time, T_w, must be >100 fs, based on the time scale of the fast components of the triexponential fits to the TIP4P and SPC/E TCFs (see Table 1). The 400-fs component that we extracted from the vibrational echo peak-shift measurement is sufficiently long that we believe it accurately reflects the characteristic time scale of decay in the TCF. Therefore, in the fitting procedure, three parameters were allowed to vary independently—the preexponential factors of two of the components and the time constant of the slowest component.

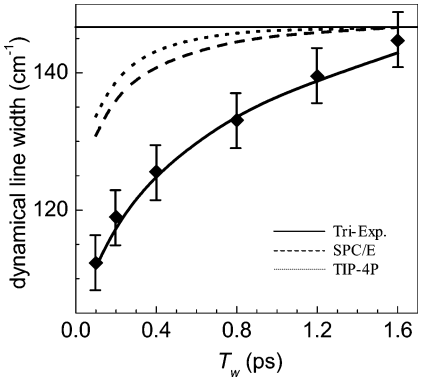

Figure 6. Comparison of the dynamical line widths of the phenomenological triexponential fit (solid line through the data) and experimental correlation spectra (diamonds with error bars) obtained from the 2D Gaussian fits. In addition, the TIP4P (dots) and SPC/E (dashes) dynamical line widths are shown. The horizontal line at 147 cm^{-1} is the long-time asymptotic line width. The triexponential phenomenological TCF does a good job of reproducing the data (see Table 1 for parameters).

The dynamical line widths extracted from the correlation spectra calculated from the phenomenological TCF are displayed in Figure 6 as the line through the experimental data. Also shown in Figure 6 are the TIP4P and SPC/E calculations displayed in Figure 5. In contrast to the TCFs derived from the water models, the TCF obtained from the fit has the correct value at 100 fs and passes through the data points within experimental error. Although the TIP4P model correlation spectra have reached their asymptotic value by 1.6 ps and SPC/E correlation spectra are close to the asymptotic value, the data and the correlation spectra obtained from the fit are still removed from the asymptotic value and are approaching it relatively slowly.

The normalized phenomenological TCF that provided the best fit to the experimental dynamical line widths using steps (3) and (4) is displayed in Figure 7, along with the TCFs obtained from MD simulation for comparison. The parameters of the phenomenological TCF are listed in Table 1. The best least-squares fit through the experimental data gives a 1.8-ps time constant for the slow component. We estimate upper and lower bounds of ± 0.5 ps based on a factor of 2 increase in the sum of the squares of the residuals.

A comparison of the phenomenological TCF with those derived from MD simulation demonstrates that the TIP4P and SPC/E models of water describe well the fast fluctuations in water but not the slower fluctuations. The fast components of the MD-derived TCFs comprise approximately half of the total decay amplitude. This feature is reproduced in the phenomenological TCF, even though this amplitude was allowed to vary independently in the fit. The two important differences between the MD-derived TCFs and the phenomenological TCF are the amplitude and time scale of the slow component. The TIP4P model essentially misses the slow component. The SPC/E model

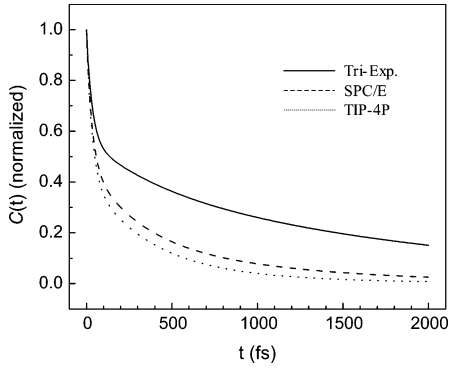

Figure 7. Comparison of the phenomenological TCF with the MD simulation-derived TCFs. The MD simulation-derived and phenomenological TCFs share a fast component comprising ~50% of the amplitude. The MD-derived TCFs differ from the phenomenological TCF in the amplitude and time scale of the slowest component.

TABLE 2: Spectral Widths of Different TCF Components

TCF	fast (decay time)	intermed. (decay time)	slow (decay time)
tri-exp. fit	48 cm^{-1} (32 fs)	38 cm^{-1} (400 fs)	111 cm^{-1} (1.8 ps)
SPC/E	48 cm^{-1} (31 fs)	97 cm^{-1} (280 fs)	88 cm^{-1} (0.98 ps)
TIP4P	56 cm^{-1} (32 fs)	115 cm^{-1} (340 fs)	50 cm^{-1} (0.90 ps)

does better but overestimates the magnitude of the intermediate and underestimates the magnitude of the slow components. In addition, the SPC/E model underestimates the time scale of the slow component by a factor of ~2. These differences in the TCFs are clearly displayed in Figure 7.

Comparing the amplitude factors of the normalized TCFs can be somewhat misleading because the fast components are motionally narrowed ($\Delta_0\tau_0 \approx 0.3-0.4$ for all of the TCFs, see Table 1). As a result, the contributions of the various components to the extent of the frequency fluctuations as observed in the dynamical line width cannot simply be compared by looking at the magnitude of Δs for each component. An alternative method is to calculate the contribution of each component to the linear line shape. We calculated the contributions to the fwhm of each component; the results are in Table 2. The fast components are mostly Lorentzian in shape because they are motionally narrowed, and the intermediate and slow components are well described by Gaussian shapes. It is important to note that the sum of the widths of the components will *not* equal the linear line width of 162 cm^{-1} because the linear line shape is the convolution of the three components. The total linear line shapes calculated from each TCF have the appropriate line width and are displayed in Figure 3. Although the fast component comprises ~50−60% of the decay in the TCFs, it contributes only a relatively small width to the total linear line shape because these components are motionally narrowed. The fast component of each TCF contributes a similar width to the linear line shapes, which is consistent with the comparison of the TCFs in Figure 7. The comparison of the TCFs in Table 2 emphasizes the relatively small contribution of the fast component and the differences in the contribution of the slow component to the linear line shape. The phenomenological TCF obtained from the triexponential fit of the data predicts the linear line shape to be dominated by the slowly varying ~1.8-ps component.

The TCF is related to the structural correlation function describing the evolution of hydrogen bonds in water because the hydroxyl stretch is sensitive to the number and strength of hydrogen bonds.[12,13,54] The relationship between frequency and structure observed through the lens of MD simulation enables us to correlate specific motions of water with components of the TCF. The calculation of the TCF from the first method using the TIP4P model has been described in detail for the OH stretch of the HOD/D_2O system.[12,13,54] In the analysis, the fast component of the TCF was assigned to hindered translational motion of hydrogen bonds (stretching of the hydrogen bond length coordinate), although there is some contribution from hydrogen bond bending.[8,12,13,55] This assignment was based on the observation of a shallow oscillation of about 1 cycle in the TCF with a period that corresponds to the estimated period of hindered translational motion of hydrogen bonds in water.[12] The oscillation is also present to varying amplitudes in the TCFs obtained for the HOD/H_2O system.[79] Calculations of the vibrational echo peak shift performed assuming δ-function pulse durations displayed an oscillation similar to that appearing in the TCF.[81] However, calculations of the vibrational echo peak shift using 50-fs pulses do not show an oscillation because the duration of the pulses is comparable to the period of the oscillation and the oscillation in the TCF is very shallow. This is consistent with electronic photon echo peak-shift calculations.[88] The TCFs shown in Figures 2 and 7 from the water models do not display the oscillation because they are the triexponential fits to the TCFs. The triexponential fits do not reduce the accuracy of subsequent calculations of the correlation spectra because the oscillations in the TCFs are not experimental observables with finite pulse durations. However, it should be recognized that the triexponential fit represents the TCF but the individual exponentials do not necessarily reflect different processes in the liquid. A true analytical form for the TCF is not known.

Assuming that the same physical interpretation holds for the HOD/H_2O system as for HOD/D_2O, the fast component of the TCFs mainly reflects the time scale of fluctuations in the hydrogen bond length coordinate. In the phenomenological TCF that fits the data, we assumed that the fastest decay constant was the same as those obtained from the MD simulations of the water models. It was possible to fit the data with this assumption, and the resulting amplitude from the fit was only slightly smaller than that obtained from the SPC/E model. This suggests that the simulation is reasonable on the shortest time scale.

In the phenomenological triexponential TCF obtained from fitting the data, there is a medium time-scale component of 400 fs that was obtained from peak-shift measurements. This value was used to limit the number of fitting parameters. It has low amplitude (16%), and it may be a crossover between the fast component and a nonexponential slower portion of the dynamics. The slower portion of the TCF calculated for the HOD/D_2O system has been assigned to the influence of hydrogen bond breaking and formation. This assignment was based on the similarity of the time constants between the slow component of the TCF and that of the hydrogen bond population correlation function.[8,12,55] The hydrogen bond population correlation function depends on the rate of hydrogen bond breaking *and* formation. The definition of the existence of a hydrogen bond is in terms of the oxygen−oxygen distance, the oxygen−hydrogen distance, and the angles involved.[91] The experimental results demonstrate that the time scale obtained from the water models is too fast and that this component of the dynamics has too little amplitude to describe the dynamics that we observe in water. Nonetheless, it is likely that the slowest time scale component is due to hydrogen bond making and breaking dynamics, but the TIP4P and the SPC/E models do not properly describe it. Additional experimental and theoretical results

indicate that hydrogen bond breaking and formation occur on the ~2 ps or longer time scale. Experiments on methanol oligomers directly measured the hydrogen bond breaking time constant and found ~2 ps.[28,29] Some MD simulations report hydrogen bond lifetimes of ~2 ps.[92,93] Although hydrogen bond breaking alone does not cause the decay of the TCF but rather the equilibration of the hydrogen bonds through both breaking and formation, the fact that hydrogen bonds break on the ~2-ps time scale suggests that they may also reach equilibrium on a similar time scale.

In fact, the slow time scale component obtained from the measurements could be longer than 2 ps. Because the TCF decays on multiple time scales, we cannot necessarily assume a form of the long-time portion of the TCF (say exponential decay) based on the measurement of T_w delays of $\leq$1.6 ps. The actual form of the long-time decay may not be exponential, which means that the 2-ps component we obtain from data collected out to $T_w = 1.6$ ps may underestimate the longest decay dynamics. Although studying the OD stretch of HOD in H_2O allows us to extend the time regime over which we measure the dynamics in water because of the longer vibrational lifetime,[7,9,18,30,35,56−58,60] we must probe them at still longer time. It is possible, although difficult, to take data on time scales that are long compared to the vibrational lifetime. As demonstrated by experiments on methanol oligomers, hydrogen bond breaking following vibrational relaxation after the second pulse in the three-pulse stimulated vibrational echo sequence can preserve the ground-state contribution to the signal.[23−25,45] Therefore, data can be collected at long times. However, the extent of hydrogen bond breaking that preserves the signal in methanol is much greater than in water, making the water experiments at long time more difficult. In addition, we must account for the influence of hydrogen bond breaking on the dynamics measured. Our detailed work studying hydrogen bond breaking in methanol using vibrational echo correlation spectroscopy[23−25,45,51] will enable us to account for hydrogen bond breaking and extend the time regime over which we access the TCF through vibrational echo correlation spectroscopy.

D. Comparison with Other Work. The dynamics in water have been addressed by other ultrafast IR techniques.[7,16−19,21,22,27,30,50,59] The closest experimental technique that measures the absorptive dynamical line shape is transient hole burning (THB).[7,16−19,21] Using THB, the dynamical line width is measured in the frequency domain, which limits the inherent time resolution of the experiment because of the time−bandwidth product of the pump and probe pulses. In systems with a clear separation of time scales between fast and slow fluctuations, the Kubo model limit,[94] the time−bandwidth product does not significantly affect the measurement if the pulses are appropriately adjusted. However, the dynamics in water are not well described by this limit.[80] Using vibrational echo correlation spectroscopy, we find that the dynamical line shape that we observe more directly accesses the dynamics in water because we avoid the complicating convolution with the spectra of the pump and probe pulses. By measuring the absorptive contribution to the dynamical line shape, we observe that vibrational echo correlation spectroscopy is more sensitive to spectral diffusion than its absolute value vibrational echo counterpart[50] because the spectral resolution is higher and interferences between ground- and excited-state features can be separated.[43] Therefore, vibrational echo correlation spectroscopy provides the most sensitive probe of the hydrogen bond dynamics in water by removing the interference from the 1−2 transition while also providing sufficient time resolution and spectral breadth to observe the global frequency fluctuations and minimizing complications from the time−bandwidth product limitation of THB.

Many experimental studies have focused on the OH stretch of HOD in D_2O,[7,16−19,21,22,27,50,59] although a recent study has focused specifically on the OD stretch of HOD in H_2O.[30] As discussed above (see section III.A), the vibrational lifetime of the OH stretch, <1 ps,[7,9,18,35,60] limited the time window of the studies that employed the OH stretch of HOD as the probe of hydrogen bond dynamics. Consequently, the experimental studies were sensitive only to the hydrogen bond dynamics of water (not the photoproducts) on the <1-ps time scale, which made the elucidation of the slower hydrogen bond fluctuations very difficult. Compared with the triexponential fit TCF presented above, most of the studies reported a faster time scale for the slow fluctuations. Much of the work utilized THB spectroscopy.[7,16−19,21,30] From these studies, the TCF was reported to decay exponentially on the 500-fs,[21] 700-fs,[7,16,17] or 1-ps[18,19] time scale. Recently, two- and three-pulse vibrational echoes have been utilized,[22,27,50,59] generally finding bi- or triexponential behavior with a fast component of 130 fs,[50] 75 fs,[59] or 33 fs[27] and a slow component of ~900 fs,[50] 1.2 ps[59] or >2 ps, perhaps as large as 5−15 ps.[22]

The transient hole-burning studies were primarily sensitive to the intermediate component of the TCF but not to the fast or slow components. The fast component (~30 fs)[8,12,13,27,54] decayed completely within the pulse duration of the pump and probe pulses (≥200-fs cross correlation in all THB studies)[7,16−19,21,30] and simply contributed to the minimum dynamical line width. Because none of the studies employed probe pulses with sufficient spectral width to measure the spectral diffusion dynamics across the entire 0−1 transition,[7,16−19,21,30] they were unable to detect the slowest frequency fluctuations. The limitation caused by too narrow a probe spectrum can be understood in the following way. To measure the time scale for the transient hole to grow to the full linear line width, it is necessary to be able to measure the full linear line width. In the previous pioneering THB studies on water,[7,16−19,21,30] the investigators frequency integrated the probe and then tuned its central frequency to piece together the THB spectrum of the $0-1$[7,16−19] and $1-2$[18,19] transitions. The spectral diffusion dynamics were extracted using this technique by constructing a model that could describe the ensemble of many separate kinetics traces collected at different wavelengths. Alternatively, the probe can be dispersed in a monochromator to frequency resolve the THB signal and measure the shift and width of the dynamical line,[26] which can be a more sensitive technique because the dynamical line is measured directly, making the extraction of the dynamics less model-dependent. In either case (spectrally dispersed or not), the narrow bandwidth of the pulses makes the slower component of the spectral diffusion dynamics extremely difficult to extract from the experimental data. In contrast to the previous THB studies, we spectrally resolve the vibrational echo signal in a monochromator, which measures the ω_m axis. The ω_τ axis is obtained by a Fourier transformation of the τ time axis (time separation between pulses 1 and 2). Both frequency axes are obtained in a single experiment in which the spectral properties of the pulses are fixed throughout. With sufficient spectral breadth (>400 cm^{-1}) because of the 45-fs pulses, we are able to span the entire 0−1 transition of water to observe the full range of spectral diffusion dynamics without the time−bandwidth product limitation. All of these factors make the experiments reported in this work more sensitive than those reported in previous studies to

the fluctuations of the hydrogen bond network in water, as reported by the TCF of water.

In addition to THB experiments, 1D two- and three-pulse vibrational echo studies have yielded significant insight into the form and time scales of the TCF of water.[22,27,50,59] The investigators studied the OH stretch of HOD in D_2O (with a the lifetime of <1 ps).[7,9,18,35,60] For the two-pulse echo studies, the lifetime-limited window was not an issue because the time scale of the experiment is much shorter than the vibrational lifetime. Yeremenko et al. heterodyne detected their two-pulse echo, which allowed them to access the fast and intermediate components.[50] However, the echo signal decayed on the 100-fs time scale, which made the extraction of the slow component extremely difficult. Consequently, the slowest component of the reported TCF was ~900 fs. Stenger et al. homodyne detected their two-pulse experiment,[27] making it sensitive primarily to the fast component because the signal decayed twice as fast compared with that from the heterodyne-detected experiment of Yeremenko.[50]

The three-pulse vibrational echo studies allowed the investigators to access the intermediate and slow time scale portions of the TCF on time scales of >100 fs, when the normalized TCF has decayed to $\ll 1$.[89,90] However, the <1-ps vibrational lifetime of the OH stretch of HOD in D_2O[7,9,18,35,60] complicated the observed dynamics on longer time scales.[22] In the recent work by Fecko et al.,[59] they did not take into account the rapid formation of hydrogen-bond-broken species that comes to dominate the signal for times longer than the vibrational lifetime.[23−26,28,29,45,51,56] However, Stenger et al. did take into account hydrogen bond breaking by introducing a "hot" ground state to which the excited species decay.[22] By introducing this state and assuming the hot species to have the same dephasing dynamics as the initially excited species, they were able to extend the window of their measurement significantly beyond the vibrational lifetime. As a result, they reported slow dynamics in the TCF that occurred on the 100-fs and >2-ps time scales, perhaps as long as 5−15 ps.[22] The report by Stenger et al. is the most consistent with the triexponential TCF reported in this work. However, these frequency-integrated techniques lack the ability to separate the 0−1 from the 1−2 transition, which may complicate the isolation of the TCF specific to the 0−1 transition.

IV. Concluding Remarks

The results of ultrafast heterodyne-detected multidimensional stimulated vibrational echo correlation spectroscopy with full phase information were employed to study the dynamics of water (H_2O). By using extremely short pulses (45 fs), it is possible to excite the entire very broad hydroxyl stretching band including the 1−2 transition. Multidimensional correlation spectroscopy makes it possible to explicate the spectral diffusion dynamics of the hydroxyl 0−1 stretching transition of water with great sensitivity in a comprehensive manner. The results presented here focus on time scales of >100 fs.

The vibrational echo correlation spectra (see Figure 1) display clear broadening along the ω_τ (horizontal) axis as T_w is increased. Once the contribution from the 1−2 transition is removed, a cut across the correlation spectrum through the center of the 0−1 peak (2500 cm^{-1}) reports the dynamical line width for each value of T_w. The dynamical line width of the 0−1 peak is a sensitive spectroscopic probe of the frequency fluctuations in water. The use of vibrational echo correlation spectroscopy to obtain 0−1 transition-time-dependent dynamical line widths is akin to doing a transient hole-burning experiment without the limitations of the time−bandwidth product. Interference from the dynamics of the 1−2 transition, which may have a different dephasing, is eliminated. From the analysis of the dynamical line widths, it was found that the frequency fluctuations in water occur on multiple time scales out to at least 2 ps.

Molecular dynamics simulations were used to obtain the time correlation functions (TCF) for two water models, TIP4P and SPC/E.[79] Using time-dependent diagrammatic perturbation theory with the full third-order nonlinear material response,[46−48] theoretical vibrational echo correlation spectra were calculated from the MD-derived TCFs and were compared to the data. Although the SPC/E model is somewhat better, both water models produce dynamical lines that broaden too rapidly. The slowest component of both TCFs is too fast and has too little amplitude to reproduce the data. A phenomenological TCF was obtained from a highly constrained fit of the data. The results are consistent with the MD results for the fastest times. The slowest component of the phenomenological TCF is 1.8 ps. On the basis of the MD simulation results, this slowest component is attributed to hydrogen bond breaking and formation (equilibration). As mentioned above, we are currently in the process of taking additional data at both longer and shorter times than the data presented in Figures 1, 5, and 6. The additional data will help pin down the detailed dynamics in water and will facilitate the development and testing of better water models.

Acknowledgment. We thank Professor Peter Hamm, Physikalisch Chemisches Institut, Universität Zürich, for help with the diagrammatic perturbation theory calculations. J.B.A., T.S., C.S., and M.D.F. thank the AFOSR (F49620-01-1-0018) for supporting this research and the NSF DMR (DMR-0332692) for additional support. T.S. also thanks the Emmy Noether program of the DFG for partial support. S.A.C., C.P.L., and J.L.S. thank the NSF (CHE-9816235 and CHE-0132538) for supporting this research.

References and Notes

(1) Choppin, G. R. *J. Mol. Struct.* **1978**, *45*, 39.
(2) Dore, J. C. *J. Mol. Struct.* **1991**, *250*, 193.
(3) Falk, M.; Ford, T. A. *Can. J. Chem.* **1966**, *44*, 1699.
(4) Luck, W. A. P. *Intermol. Forces* **1991**, 217.
(5) Ludwig, R. *Angew. Chem., Int. Ed.* **2001**, *40*, 1808.
(6) Bakker, H. J.; Woutersen, S.; Nienhuys, H. K. *Chem. Phys.* **2000**, *258*, 233.
(7) Gale, G. M.; Gallot, G.; Hache, F.; Lascoux, N.; Bratos, S.; Leicknam, J. C. *Phys. Rev. Lett.* **1999**, *82*, 1068.
(8) Lawrence, C. P.; Skinner, J. L. *Chem. Phys. Lett.* **2003**, *369*, 472.
(9) Woutersen, S.; Emmerichs, U.; Nienhuys, H.-K.; Bakker, H. J. *Phys. Rev. Lett.* **1998**, *81*, 1106.
(10) Mikenda, W. *J. Mol. Struct.* **1986**, *147*, 1.
(11) Novak, A. Hydrogen Bonding in Solids. In *Structure and Bonding*; Dunitz, J. D., Ed.; Springer-Verlag: Berlin, 1974; Vol. 18, p 177.
(12) Lawrence, C. P.; Skinner, J. L. *J. Chem. Phys.* **2003**, *118*, 264.
(13) Lawrence, C. P.; Skinner, J. L. *J. Chem. Phys.* **2002**, *117*, 8847.
(14) Pimentel, G. C.; McClellan, A. L. *The Hydrogen Bond*; W. H. Freeman and Co.: San Francisco, 1960.
(15) Liddel, U.; Becker, E. D. *Spectrochim. Acta* **1957**, *10*, 70.
(16) Bratos, S.; Gale, G. M.; Gallot, G.; Hache, F.; Lascoux, N.; Leicknam, J. C. *Phys. Rev. E* **2000**, *61*, 5211.
(17) Gallot, G.; Lascoux, N.; Gale, G. M.; Leicknam, J. C.; Bratos, S.; Pommeret, S. *Chem. Phys. Lett.* **2001**, *341*, 535.
(18) Laenen, R.; Rausch, C.; Laubereau, A. *Phys. Rev. Lett.* **1998**, *80*, 2622.
(19) Laenen, R.; Rausch, C.; Laubereau, A. *J. Phys. Chem. B* **1998**, *102*, 9304.
(20) Laenen, R.; Rauscher, C.; Laubereau, A. *J. Phys. Chem. A* **1997**, *101*, 3201.
(21) Woutersen, S.; Bakker, H. J. *Phys. Rev. Lett.* **1999**, *83*, 2077.
(22) Stenger, J.; Madsen, D.; Hamm, P.; Nibbering, E. T. J.; Elsaesser, T. *J. Phys. Chem. A* **2002**, *106*, 2341.
(23) Asbury, J. B.; Steinel, T.; Stromberg, C.; Gaffney, K. J.; Piletic, I. R.; Goun, A.; Fayer, M. D. *Chem. Phys. Lett.* **2003**, *374*, 362.

(24) Asbury, J. B.; Steinel, T.; Stromberg, C.; Gaffney, K. J.; Piletic, I. R.; Fayer, M. D. *J. Chem. Phys.* **2003**, *119*, 12981.
(25) Asbury, J. B.; Steinel, T.; Fayer, M. D. *J. Lumin.*, in press, 2004.
(26) Piletic, I. R.; Gaffney, K. J.; Fayer, M. D. *J. Chem. Phys.* **2003**, *119*, 423.
(27) Stenger, J.; Madsen, D.; Hamm, P.; Nibbering, E. T. J.; Elsaesser, T. *Phys. Rev. Lett.* **2001**, *87*, 027401.
(28) Gaffney, K. J.; Davis, P. H.; Piletic, I. R.; Levinger, N. E.; Fayer, M. D. *J. Phys. Chem. A* **2002**, *106*, 12012.
(29) Gaffney, K.; Piletic, I.; Fayer, M. D. *J. Phys. Chem. A* **2002**, *106*, 9428.
(30) Kropman, M. F.; Nienhuys, H.-K.; Woutersen, S.; Bakker, H. J. *J. Phys. Chem. A* **2001**, *105*, 4622.
(31) Gaffney, K. J.; Piletic, I. R.; Fayer, M. D. *J. Chem. Phys.* **2003**, *118*, 2270.
(32) Laenen, R.; Rauscher, C.; Simeonidis, K. *J. Chem. Phys.* **1999**, *110*, 5814.
(33) Laenen, R.; Simeonidis, K. *Chem. Phys. Lett.* **1999**, *299*, 589.
(34) Laenen, R.; Rauscher, C. *Chem. Phys. Lett.* **1997**, *274*, 63.
(35) Gale, G. M.; Gallot, G.; Lascoux, N. *Chem. Phys. Lett.* **1999**, *311*, 123.
(36) Zimdars, D.; Tokmakoff, A.; Chen, S.; Greenfield, S. R.; Fayer, M. D.; Smith, T. I.; Schwettman, H. A. *Phys. Rev. Lett.* **1993**, *70*, 2718.
(37) Tokmakoff, A.; Fayer, M. D. *J. Chem. Phys.* **1995**, *102*, 2810.
(38) Rector, K. D.; Fayer, M. D. *Laser Chem.* **1999**, *19*, 19.
(39) Hamm, P.; Lim, M.; Hochstrasser, R. M. *Phys. Rev. Lett.* **1998**, *81*, 5326.
(40) Zanni, M. T.; Asplund, M. C.; Hochstrasser, R. M. *J. Chem. Phys.* **2001**, *114*, 4579.
(41) Merchant, K. A.; Thompson, D. E.; Fayer, M. D. *Phys. Rev. Lett.* **2001**, *86*, 3899.
(42) Golonzka, O.; Khalil, M.; Demirdoven, N.; Tokmakoff, A. *Phys. Rev. Lett.* **2001**, *86*, 2154.
(43) Khalil, M.; Demirdoven, N.; Tokmakoff, A. *J. Phys. Chem. A* **2003**, *107*, 5258.
(44) Khalil, M.; Demirdoven, N.; Tokmakoff, A. *Phys. Rev. Lett.* **2003**, *90*, 047401(4).
(45) Asbury, J. B.; Steinel, T.; Stromberg, C.; Gaffney, K. J.; Piletic, I. R.; Goun, A.; Fayer, M. D. *Phys. Rev. Lett.* **2003**, *91*, 237402.
(46) Mukamel, S. *Annu. Rev. Phys. Chem.* **2000**, *51*, 691.
(47) Mukamel, S. *Principles of Nonlinear Optical Spectroscopy*; Oxford University Press: New York, 1995.
(48) Zhang, W. M.; Chernyak, V.; Mukamel, S. *J. Chem. Phys.* **1999**, *110*, 5011.
(49) Jonas, D. M. *Annu. Rev. Phys. Chem.* **2003**, *54*, 425.
(50) Yeremenko, S.; Pshenichnikov, M. S.; Wiersma, D. A. *Chem. Phys. Lett.* **2003**, *369*, 107.
(51) Asbury, J. B.; Steinel, T.; Fayer, M. D. *J. Phys. Chem. A*, accepted for publication, 2003.
(52) Veldhuizen, R.; de Leeuw, S. W. *J. Chem. Phys.* **1996**, *105*, 2828.
(53) zum Buschenfelde, D. M.; Staib, A. *Chem. Phys.* **1998**, *236*, 253.
(54) Lawrence, C. P.; Skinner, J. L. *J. Chem. Phys.* **2002**, *117*, 5827.
(55) Rey, R.; Møller, K. B.; Hynes, J. T. *J. Phys. Chem. A* **2002**, *106*, 11993.
(56) Asbury, J. B.; Steinel, T.; Fayer, M. D. 2003, to be published.
(57) Laenen, R.; Simeonidis, K.; Laubereau, A. *J. Phys. Chem. B* **2002**, *106*, 408.
(58) Deak, J. C.; Rhea, S. T.; Iwaki, L. K.; Dlott, D. D. *J. Phys. Chem. A* **2000**, *104*, 4866.
(59) Fecko, C. J.; Eaves, J. D.; Loparo, J. J.; Tokmakoff, A.; Geissler, P. L. *Science*, in press, 2003.
(60) Nienhuys, H.-K.; Woutersen, S.; van Santen, R. A.; Bakker, H. J. *J. Chem. Phys.* **1999**, *111*, 1494.
(61) Hybl, J. D.; Ferro, A. A.; Jonas, D. M. *J. Chem. Phys.* **2001**, *115*, 6606.
(62) Ernst, R. R.; Bodenhausen, G.; Wokaun, A. *Nuclear Magnetic Resonance in One and Two Dimensions*; Oxford University Press: Oxford, England, 1987.
(63) Jorgensen, W. L.; Chandrasekhar, J.; Nadura, J. D. *J. Chem. Phys.* **1983**, *79*, 926.
(64) Berendsen, H. J. C.; Grigera, J. R.; Straatsma, T. P. *J. Phys. Chem.* **1987**, *91*, 6269.
(65) Tokmakoff, A. *J. Phys. Chem. A* **2000**, *104*, 4247.
(66) Hybl, J. D.; Christophe, Y.; Jonas, D. M. *Chem. Phys.* **2001**, *266*, 295.
(67) Berg, M.; Walsh, C. A.; Narasimhan, L. R.; Littau, K. A.; Fayer, M. D. *J. Chem. Phys.* **1988**, *88*, 1564.
(68) Berg, M. A.; Rector, K. D.; Fayer, M. D. *J. Chem. Phys.* **2000**, *113*, 3233.
(69) Littau, K. A.; Bai, Y. S.; Fayer, M. D. *Chem. Phys. Lett.* **1989**, *159*, 1.
(70) Tokmakoff, A.; Urdahl, R. S.; Zimdars, D.; Francis, R. S.; Kwok, S.; Fayer, M. D. *J. Chem. Phys.* **1995**, *102*, 3919.
(71) Steinel, T.; Asbury, J. B.; Corcelli, S. A.; Lawrence, C. P.; Skinner, J. L.; Fayer, M. D. *Science*, submitted for publication, 2003.
(72) Lock, A. J.; Woutersen, S.; Bakker, H. J. *J. Phys. Chem. A* **2001**, *105*, 1238.
(73) Graener, H.; Ye, T. Q.; Laubereau, A. *J. Chem. Phys.* **1989**, *91*, 1043.
(74) Graener, H.; Ye, T. Q.; Laubereau, A. *J. Chem. Phys.* **1989**, *90*, 3413.
(75) Laenen, R.; Rauscher, C.; Laubereau, A. *Chem. Phys. Lett.* **1998**, *283*, 7.
(76) Laenen, R.; Gale, G. M.; Lascoux, N. *J. Phys. Chem. A* **1999**, *103*, 10708.
(77) Woutersen, S.; Emmerichs, U.; Bakker, H. J. *J. Chem. Phys.* **1997**, *107*, 1483.
(78) Polyansky, O. L.; Jensen, P.; Tennyson, J. *J. Chem. Phys.* **1996**, *105*, 6490.
(79) Corcelli, S. A.; Lawrence, C. P.; Skinner, J. L., in preparation, 2003.
(80) Piryatinski, A.; Lawrence, C. P.; Skinner, J. L. *J. Chem. Phys.* **2003**, *118*, 9664.
(81) Piryatinski, A.; Lawrence, C. P.; Skinner, J. L. *J. Chem. Phys.* **2003**, *118*, 9672.
(82) Mukamel, S.; Loring, R. F. *J. Opt. Soc. Am. B* **1986**, *3*, 595.
(83) Mukamel, S. **2003**, private communication.
(84) Hamm, P. Private communication, 2003.
(85) Hamm, P.; Lim, M.; Degrado, W. F.; Hochstrasser, R. M. *J. Chem. Phys.* **2000**, *112*, 1907.
(86) Hamm, P.; Lim, M.; Degrado, W. F.; Hochstrasser, R. M. *J. Phys. Chem. A* **1999**, *103*, 10049.
(87) de Boeij, W.; Pshenichnikov, M. S.; Wiersma, D. A. *Chem. Phys. Lett.* **1996**, *253*, 53.
(88) Joo, T. H.; Jia, Y. W.; Yu, J. Y.; Jonas, D. M.; Fleming, G. R. *J. Chem. Phys.* **1996**, *104*, 6089.
(89) Everitt, K. F.; Geva, E.; Skinner, J. L. *J. Chem. Phys.* **2001**, *114*, 1326.
(90) Piryatinski, A.; Skinner, J. L. *J. Phys. Chem. B* **2002**, *106*, 8055.
(91) Mezei, M.; Beveridge, D. L. *J. Chem. Phys.* **1981**, *74*, 622.
(92) Luzar, A. *J. Chem. Phys.* **2000**, *113*, 10663.
(93) Marti, J.; Padro, J. A.; Guardia, E. *J. Chem. Phys.* **1996**, *105*, 639.
(94) Kubo, R. A Stochastic Theory of Line-Shape and Relaxation. In *Fluctuation, Relaxation and Resonance in Magnetic Systems*; Ter Haar, D., Ed.; Oliver and Boyd: London, 1961.